Fluorescent nanopigments: Quantitative assessment of their quantum yield

R. Ferrini,[1,a)] O. Nicolet,[1,b)] S. Huber,[1,c)] L. Zuppiroli,[1] S. Chappellet,[2,d)] C. Lovey,[2] J. Perrenoud,[2] and M. Pauchard[2,e)]
[1]*Lab. d'Optoélectronique des Matériaux Moléculaires (LOMM), Ecole Polytechnique Fédérale de Lausanne (EPFL), Station 3, CH-1015 Lausanne, Switzerland*
[2]*ILFORD Imaging Switzerland GmbH, R.te de l'Ancienne Papeterie, C.P. 160, CH-1723 Marly, Switzerland*

(Received 8 February 2010; accepted 9 March 2010; published online 14 June 2010)

In the last few years, an intense research effort has focused on the synthesis of fluorescent nanopigments for functional inks, light harvesting, tagging, tracing, (bio)labeling, imaging, and lighting applications. Moreover, combined with dielectric matrices, these fluorescent nanoparticles may open the way to the realization of novel optophotonic devices. In particular, due to the large variety of available organic fluorescent dyes, their encapsulation into either an inorganic or an organic host is a very promising approach to synthesize a large palette of new fluorescent nanopigments. However, since the dye encapsulation may affect the fluorescence efficiency, measuring the quantum yield of fluorescent nanopigments is of paramount importance for the development of any connected application. In this article, we present a diffuse reflectance (DR) technique that enables the quantitative assessment of the quantum yield of fluorescent nanoparticles such as zeolite L nanocrystals and poly(methyl methacrylate) nanospheres both loaded with fluorescent perylene molecules. Our method is validated by measuring a well known fluorescence standard and by comparing the results obtained for a model zeolite nanopigment with those provided by an alternative DR technique. Reliable and reproducible quantum yield values are obtained for both low- and high-efficiency fluorescent nanoparticles. Our technique can thus enable systematic and quantitative studies that may yield an important insight in the mechanisms affecting the fluorescence efficiency of a large variety of nanopigments. © *2010 American Institute of Physics*. [doi:10.1063/1.3387891]

I. INTRODUCTION

In the last decade, nanopigments have been intensively studied as novel fluorescent materials for functional inks, light harvesting, tagging, tracing, biolabeling, imaging, and lighting applications.[1–8] Moreover, functionalizing the external surface of the these fluorescent nanoparticles and embedding them into a dielectric (e.g., polymer) matrix has enabled the realization of a large variety of novel optophotonic devices.[9–14] Recently, due to the wealth of existing organic fluorescent dyes, their encapsulation into either an inorganic or an organic host has been demonstrated to be a very promising and versatile approach to synthesize a large palette of new fluorescent pigments. In particular, both organic-inorganic[14–16] and organic-organic[17–19] host-guest nanosystems have been extensively developed for the chemical, photochemical or thermal stabilization and the supramolecular organization of organic fluorescent dye molecules, complexes, and clusters.[19–25] The most common examples of such systems are

(i) *nanoporous zeolites*: besides their widespread commercial use as catalysts and ion-exchangers,[26] due to their nanoporous framework consisting of nanochannels with a minimal diameter of several angstrom, they have been used as inorganic hosts for the encapsulation of different organic molecules,[2,20–22,27–31]
(ii) *mesoporous silica particles*: because of their uniform porosity, they have been recently proposed as promising inorganic hosts with an adjustable pore size in the range of 1–10 nm,[32–35]
(iii) *silica nanoparticles*: once loaded with fluorescent organic dyes, these inorganic nanohosts have been shown to possess interesting physical-chemical and photochemical properties,[36–40]
(iv) *fluorescent polymer nanoparticles*: as stable organic hosts, they have attracted both research[6,8,17–19,23,25,41] and commercial[42] interest for the development and the fabrication of novel functional materials;
(v) *organic-organic supramolecular complexes*: they have been developed using organic macromolecules as hosts that can encapsulate small organic molecules or ions.[43,44]

Due to their high versatility, these host-guest systems offer a wide range of possibilities for preparing nanopigments with tailored chemical and physical properties. Nevertheless, we observe that, since the host-guest interactions can strongly affect the dye fluorescence efficiency, measuring the quantum yield of both organic-inorganic and organic-organic fluorescent nanoparticules is of paramount importance for the development of any optophotonic application. Unfortu-

[a)]Electronic mail: rolando.ferrini@epfl.ch.
[b)]Present address: Nestlé Product Technology Centre NESTEC Ltd, CH-1350 Orbe, Switzerland.
[c)]Present address: Merz+Benteli AG, CH-3172 Niederwangen, Switzerland.
[d)]Present address: Rolic Technologies Ltd., CH-4123 Allschwil, Switzerland.
[e)]Present address: Adolphe Merkle Institute-University of Fribourg, CH-1723 Marly, Switzerland.

nately, although the optical properties and the fluorescence efficiency of most organic dyes are reported in the literature[45] and/or can be easily measured in solution,[46,47] very few systematic and quantitative studies on the quantum yield of fluorescent nanopigments can be found in the literature[18,19] and a precise measurement is often lacking. On one hand, the *relative* quantum yield is indeed commonly estimated by comparison with a well-know fluorescent agent in solution taken as reference.[18,19,25,48,49] Since the emission can be assumed to be isotropic, the relative method works well for liquid samples, provided that the sample and the reference have an identical concentration yielding an identical absorption. However, for organic-inorganic and organic-organic nanopigments, when the particle size is larger than 100 nm, their morphology strongly affects both emission and absorption due to light scattering and self-absorption. It is clear that a proper reference sample should closely resemble those morphological properties. Nevertheless, it is nearly impossible to find such a reference for all fluorescent nanopigments. Using a standard that poorly simulates the anisotropic fluorescence of the studied material will lead to large errors in the resulting quantum yield values and extrinsic corrections will be necessary.[25] On the other hand, either complex techniques such as the thermal lens effect,[50] or emission/absorption measurements in solution or in transparent films,[51] or integrating sphere measurements on thin films[52] are used to indirectly assess the *absolute* quantum yield without the need for a standard reference.[40] But again, light scattering and self-absorption become critical for nanoparticles with sizes in the order of several hundreds of nanometers. Therefore, a direct and reliable absolute measurement is of paramount importance to enable systematic and quantitative studies of the quantum yield of fluorescent nanopigments.

In this article, we present an optical technique that allows the direct measurement of the *absolute* quantum yield of fluorescent nanoparticles such as zeolite L (ZL) nanocrystals[2,20–22,28–31] and poly(methyl methacrylate) (PMMA) nanospheres[5,17,19,23–25,53,54] both loaded with fluorescent perylene molecules, which are well known for their chemical and photochemical stabilities as well as for their high quantum yield.[5,55] Our experimental method is based on the measurement of the diffuse reflectance (DR) spectra of fluorescent nanopigments adsorbed on microcrystalline cellulose substrates. In particular, we adapted the DR technique previously developed by Ruetten and Thomas[56] and Ferreira *et al.*[57] for the measurement of the fluorescence efficiency of organic dyes to the assessment of the quantum yield of organic-inorganic and organic-organic nanopigments, for which both light scattering and self-absorption strongly affect the fluorescence emission. To this purpose, an optical bench was equipped with a standard lamp-monochromator system and a calibrated integrating sphere coupled to a photodetector, which eventually eliminates any influence of the nanoparticle emission anisotropy on the optical measurements. Our technique was validated (*i*) by measuring a well known fluorescence standard (Rhodamine 101) and (*ii*) by comparing the results obtained for a model zeolite nanopigment with those provided by an alternative DR technique by Rohwer and Martin.[58] Finally, reliable and precise quantum yield values were obtained for both low- and high-efficiency fluorescent nanoparticles, i.e., for both perylene-loaded zeolite nanocrystals and PMMA nanospheres, respectively.

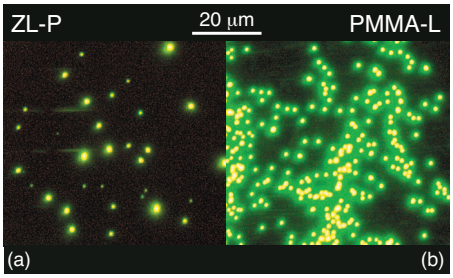

FIG. 1. (Color) Fluorescence microscopy images of (a) 200 nm zeolite L nanocrystals (ZL–P) and (b) 300 nm PMMA nanospheres (PMMA–L) loaded with perylene molecules, i.e., 3,9-perylenedicarboxylic acid diisobutyl ester (PDB: see the inset of Fig. 2) and Lumogen F Yellow 083 (LY83: see the inset of Fig. 3), respectively.

II. MATERIALS

Fluorescence microscopy images of ZL and PMMA nanopigments are shown in Fig. 1. They were taken by imaging a drop of the nanoparticle dispersion with an Olympus BX61 optical microscope equipped with a 100 W mercury discharge lamp, an excitation filter centered at 450 nm, and a long-pass emission filter with a cut-on wavelength located at 520 nm. These nanopigments were synthesized by loading either the inorganic or the organic host with fluorescent perylene dyes (organic guest).[5,55] Before the encapsulation of the dye molecules, their purity was checked by standard analysis methods (e.g., NMR) that yielded negligible impurity concentrations for all the used products. Moreover, we made a few tests with perylene molecules purified by gradient sublimation but we did not find any difference in the optical properties of the fluorescent nanoparticles after the host loading.

A. Zeolite L fluorescent nanocrystals

ZL nanocrystals consist of cylindrically shaped aluminosilicate nanoporous nanoparticles with one dimensional channels with a minimal diameter of 7 Å running along the crystal axis.[2] ZL nanoparticles with an aspect ratio of 1:1 and a narrow size distribution around 200 nm were synthesized using a hydrothermal process.[59] Details on the synthesis procedure and parameters can be found in Ref. 60.

3,9-Perylenedicarboxylic acid diisobutyl ester (PDB; see the inset of Fig. 2) molecules by ABCR (Ref. 61) were infiltrated into the zeolite channels with a gas-phase method at 180 °C thus obtaining ZL–P organic-inorganic nanopigments [see Fig. 1(a)].[22,62,63] Note that, in order to perform DR measurements, the ZL–P nanoparticles are adsorbed into microcrystalline cellulose substrates using a solvent evaporation method under heating and reduced pressure (see below). Therefore, in order to guarantee the nanopigment stability (i.e., to prevent the leakage of the neutral dye molecules), a well-known plugging method was adopted.[64] We observed that the emission spectrum of the modified ZL–P nanopigments perfectly agrees with the spectrum of

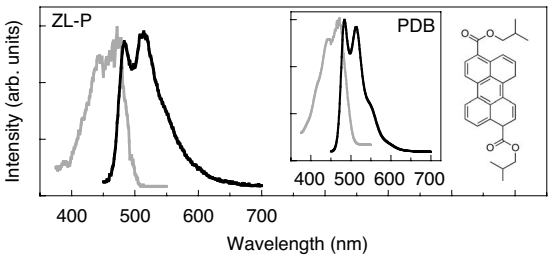

FIG. 2. Steady-state excitation (gray lines) and emission (black lines) spectra of ZL–P nanoparticles dispersed in toluene (concentration=5 mg/l). In the inset, the structure and the spectra of the PDB molecules in solution (concentration in toluene=10^{-6} M) are shown as reference. For the excitation and the emission spectra, the emission was collected at 560 nm and the excitation was set at 440 nm, respectively.

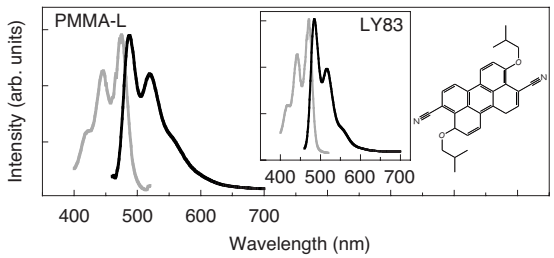

FIG. 3. Steady-state excitation (gray lines) and emission (black lines) spectra of PMMA–L nanospheres dispersed in water (concentration=38 g/l). In the inset, the structure and the spectra of the LY83 molecules in solution (concentration in ethanol=5×10^{-5} M) are shown as reference. For the excitation and the emission spectra, the emission was collected at 530 nm and the excitation was set at 450 nm, respectively.

the bare ZL–P nanoparticles before the adsorption of the plugging agent at the channel entrances. A thorough description of the infiltration technique as well as the plugging procedure and the loading stability tests is given in Ref. 60. The loading efficiency was estimated by selectively dissolving the inorganic zeolite framework with hydrofluoric (HF) acid and then measuring the solution absorption spectrum (see Ref. 60 for details). Comparing with the absorption spectrum of reference solutions, the exact quantity of PDB molecules loaded into the ZL–P nanopigments [in milligram per gram (mg/g)] was obtained and the corresponding concentration in solution [in Mole per liter (Mol/l)] was calculated.

B. PMMA fluorescent nanospheres

Monodisperse PMMA nanospheres[53] were synthesized by surfactant-free microemulsion polymerization with potassium peroxodisulfate as initiator.[17,65] The monomer and the initiator concentrations were adjusted to obtain nanoparticles with an average size in the order of 300 nm. The polymer solution was purified from large agglomerates and from low molecular impurities by filtration and centrifugation, respectively. The nanoparticle size was characterized using a CPS disk centrifuge, a narrow size distribution around 310 nm was obtained.

After the polymerization, postsynthesis swelling was adopted to load the PMMA nanoparticles with perylene molecules.[54] In particular, an organic solvent [i.e., tetrahydrofuran (THF)] was used to swell the PMMA nanospheres suspended in an aqueous solution in order to load them with a commercial fluorescent dye, the Lumogen F Yellow 083 (LY83; see the inset of Fig. 3) by BASF.[66] Finally, the solvent was evaporated under reduced pressure to leave the LY83 molecules encapsulated into the beads, thus obtaining PMMA–L organic-organic nanopigments [see Fig. 1(b)]. Similarly to the technique adopted for ZL–P nanopigments, the dye concentration was estimated by (*i*) dissolving the loaded PMMA nanospheres in THF, (*ii*) measuring the solution absorption spectrum, and (*iii*) comparing with the absorption spectrum of reference solutions. The exact quantity of LY83 molecules loaded into the PMMA–L nanopigments (in mg/g) was thus obtained and the corresponding concentration in solution (in Mol/l) was calculated.

III. SAMPLES

A. Sample preparation

1. Dye solutions and nanopigment dispersions for optical characterization

PDB (LY83) solutions and ZL–P (PMMA–L) dispersions were prepared for the optical characterization of both dyes and nanopigments (see below). Ethanol (Fluka, HPLC grad) and toluene (Acros, spectrophotometric grade) were used for the PDB and LY83 solutions, respectively. The molecules were highly diluted (PDB=10^{-6} M; LY83=5×10^{-5} M) in order to minimize the formation of aggregates. ZL–P and PMMA–L were dispersed in toluene (5 mg/l) and in water (38 g/l), respectively.

2. Cellulose samples for diffused reflectance measurements

Cellulose samples loaded with ZL–P and PMMA–L nanopigments were prepared for DR measurements by adsorbing the fluorescent nanoparticles onto microcrystalline cellulose substrates characterized by high DR (i.e., $\geq$80%) in the visible spectral region. The high porosity of such substrates enables a very good dispersion of the fluorescent nanopigments in the cellulose matrix. Following a solvent evaporation procedure,[57] the nanopigment dispersions were mixed with the powdered substrate and the solvent was subsequently evaporated, thus leaving the fluorescent nanopigments adsorbed onto the cellulose substrate.[67] The microcrystalline cellulose (Fluka DS-O) was previously dried at a temperature of 60 °C and a pressure of 450 Torr for 3 h. The temperature must be kept below 70 °C in order to avoid cellulose degradation and, thus, a decrease in the substrate DR. ZL–P and PMMA–L dispersions were prepared in a 1:1 mixture of ethanol (Fluka, HPLC grade) and toluene (Acros, spectrophotometric grade) and in water, respectively, with different nanopigment concentrations. In the case of ZL–P, the mixture composition was optimized in order to obtain good nanoparticle dispersion and adsorption, thus improving the spatial homogeneity of the loaded cellulose samples. An ultrasonic bath was used for 30–40 min to homogenize the dispersions that were then mixed with the microcrystalline cellulose in a 1 ml/500 mg proportion. For the ZL–P, the solvent was slowly evaporated during 2 h in a fume hood, while 20 s of ultrasonic bath were applied every 10 min to

achieve a better dispersion of the nanoparticles in the cellulose. The residual solvent was eventually removed by heating the sample overnight at a temperature of 60 °C under moderate vacuum (450 Torr). For the PMMA–L nanopigments, the samples were dried at a temperature of 50 °C under moderate vacuum (450 Torr) for 168 h. After the solvent evaporation, the fluorescent powders were placed in a powder holder suitable for measurements in the integrating sphere. We remark that the samples prepared for the same set of measurements were always processed together in order to guarantee the same optical properties for all substrates.

B. Sample characterization

The steady-state excitation and emission spectra of both dye and nanopigment dispersions were measured with a standard fluorimeter (Horiba Jobin-Yvon Fluoromax-3). In the case of the cellulose samples, a fluorimeter (Varian Cary Eclipse) equipped with an optical fiber was used.

1. Zeolite L fluorescent nanocrystals

The steady-state excitation (gray line) and emission (black line) spectra of ZL–P nanopigments (dye concentration=1.70 10^{-1} Mol/l) dispersed in a toluene solution (content=5 mg/l) are shown in Fig. 2. For the excitation spectrum, the emission was collected at 560 nm, while, for the emission spectrum, the excitation was performed at 440 nm. On one hand, the spectral location of the emission features in the ZL–P fluorescence spectrum well agrees with that observed in the PDB spectrum (see the inset in Fig. 2). On the other hand, the change of the overall spectral shape shows that the encapsulation in the inorganic host does indeed affect the dye fluorescence: for instance, the aggregate-related shoulder that appears at 560 nm in the PDB emission becomes negligible in the ZL–P spectrum (see Ref. 60 for details), thus confirming that the infiltration in the zeolite nanochannels prevents the dye molecules from aggregation.[2]

2. PMMA fluorescent nanospheres

The steady-state excitation (gray line) and emission (black line) spectra of the PMMA–L nanoparticles (dye concentration=6.38 10^{-3} Mol/l) dispersed in a water solution (content=38 g/l) are shown in Fig. 3. For the excitation spectrum, the emission was collected at 530 nm, while, for the emission spectrum, the excitation was performed at 450 nm. As for ZL–P, the spectral location of the emission features in the PMMA–L fluorescence spectrum well agrees with that observed in the LY83 spectrum (see the inset in Fig. 3). Note that, in order to avoid aggregate formation, the dye concentration in the PMMA nanospheres must be kept much lower than in the ZL nanoparticles and, consequently, the PMMA–L content in the dispersion is several orders of magnitudes larger than the ZL–P content. Nevertheless, contrary to ZL–P nanopigments, the aggregate-related shoulder that appears at 560 nm in the LY83 emission does not disappear in the PMMA–L spectrum, thus showing the presence of a very small quantity of residual aggregates in the PMMA nanoparticles.

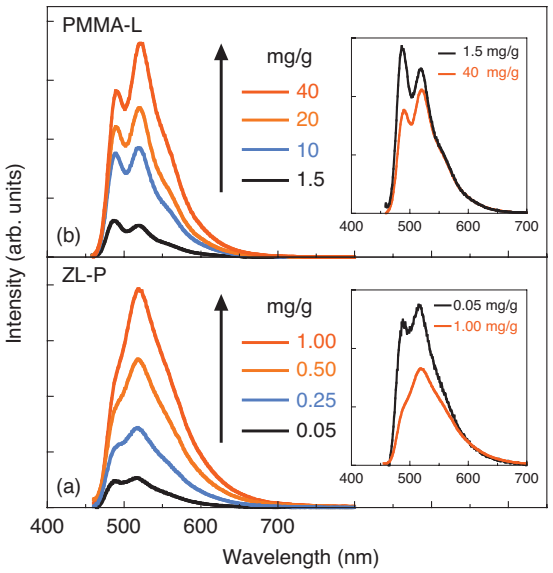

FIG. 4. (Color) Steady-state emission spectra of (a) ZL–P and (b) PMMA–L nanopigments adsorbed onto microcrystalline cellulose for increasing nanoparticle contents [in mg (nanoparticle)/g (cellulose)]. In the insets, the spectra for the lowest and the largest nanoparticle concentrations (0.05–1.00 mg/g and 1.5–40 mg/g for ZL–P and PMMA–L, respectively) have been normalized at 600 nm (where self-absorption is absent: see Figs. 2 and 3) for a better comparison of their spectral shape.

3. Fluorescent cellulose samples

The emission spectra of the ZL–P and PMMA–L nanopigments adsorbed on the cellulose substrates are shown in Figs. 4(a) and 4(b), respectively, for an increasing nanoparticle content. The samples were prepared choosing the nanoparticle to cellulose weight proportions (in mg/g) to guarantee an absorption value in the order of 1%–15% at the excitation wavelength. Note that, as for the dispersions for emission/absorption measurements, due to the lower dye concentration in the PMMA nanospheres than in the ZL nanocrystals, the PMMA–L content in the cellulose is several orders of magnitudes larger than the ZL–P content. In the insets of Fig. 4, the emission spectra for the lowest and the largest nanopigment concentrations (0.05–1 mg/g and 1.5–40 mg/g for ZL–P and PMMA–L, respectively) are normalized at 600 nm (where self-absorption is absent: see Figs. 2 and 3) for a better comparison of their spectral shape. We observe that, while for the lowest concentration values, both the ZL–P and PMMA–L spectra well agree with the corresponding spectra measured in solution (see Figs. 2 and 3), for the largest values the spectra are strongly affected by the increasing nanopigment content. On one hand, as it is expected intuitively, the emission intensity linearly increases with the increasing nanoparticle content. On the other hand, since for both PDB and LY83, as well as for the corresponding ZL–P and PMMA–L nanopigments, the Stokes shift is small (see Figs. 2 and 3), the spectral shape changes due to self-absorption effects.[57,68,69]

IV. THE DIFFUSE REFLECTANCE TECHNIQUE

Based on previous studies by Ruetten and Thomas[56] and Ferreira *et al.*,[57] we developed an optical DR technique to measure the *absolute* quantum yield of fluorescent nanopig-

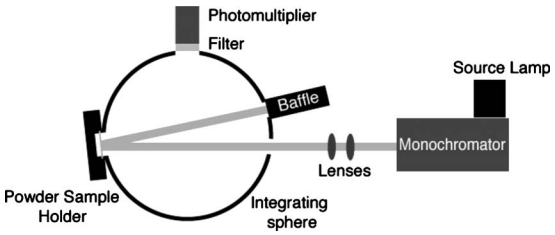

FIG. 5. Sketch of the experimental setup used for DR measurements.

ments. The DR spectra of fluorescent nanopigments adsorbed on microcrystalline cellulose substrates were measured using the integrating-sphere setup described below (Sec. IV A). The experimental technique and the data analysis procedures were adapted to the specific properties of fluorescent nanopigments and generalized to be applied to any optical setup (Sec. IV B).

A. Experimental set-up

The DR measurements were performed by means of the optical bench illustrated in Fig. 5 and consisting of an integrating sphere (Oriel, model n. 70679) coupled to a standard halogen lamp (12 V, 100 W) mounted on a computer-controlled monochromator (Jobin Yvon, model n. HR460). A lens system was used to focus the monochromatic visible light beam through the sphere aperture directly onto the sample (spot diameter=6–8 mm). The sample was placed in a powder holder fixed on a thin 1 in. quartz window. The specular component of the sample-window reflectance was eliminated using a baffle. Cut-on filters (Edmund Optics, model n. 47287 for PDB) were selectively introduced in front of the photodetector (Hamamatsu photomultiplier, model n. R928) in order to prevent the fluorescence emission from being detected. The detection system (integrating sphere+photodetector) was calibrated using barium sulfate (Fluka, purum) and carbon particles (Cabot 2000) as perfect reflector (i.e., $R \approx 1$) and black standard (i.e., $R \approx 0$), respectively. The reflectance spectra were recorded for excitation wavelengths ranging from 300 to 800 nm.

B. Quantitative assessment of the quantum yield

Following Ferreira *et al.*,[57] the quantitative assessment of the *absolute* (dye) nanopigment quantum yield was achieved shining a monochromatic light beam on the loaded cellulose substrates and recording the DR intensity at different excitation wavelengths. When this latter wavelength falls in the (dye) nanopigment absorption region, the DR signal consists of two independent components: the (dye) nanopigment emission combines with the main contribution given by the diffused excitation beam. On one hand, due to the (dye) nanopigment absorption, the intensity of the excitation background strongly decreases with respect to the bare cellulose substrates. On the other hand, the DR of the loaded samples is usually measured in two different experimental configurations, i.e., with and without a cut-on filter in front of the detector, thus yielding two different DR spectra, R_f and R_{wof}, respectively. Since the cut-on filter prevents the nanopigment fluorescence from being detected, R_{wof} is always larger than

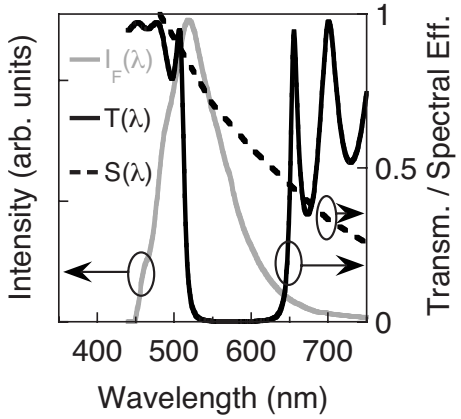

FIG. 6. $I_F(\lambda)$: steady-state emission spectrum of ZL–P nanoparticles (gray line). $T(\lambda)$: residual transmission through the cut-on filter (black solid line). $S(\lambda)$: photodetector spectral efficiency (black dotted line).

R_f and, intuitively, this difference is proportional to the nanopigment quantum yield: the larger is the fluorescence efficiency the larger will be the difference. Finally, as it is shown in details in the following, by introducing a few correction factors taking into account both the detector and the filter spectral responses, as well as, if necessary, the (dye) nanopigment self-absorption, the *absolute* quantum yield can be quantitatively assessed.

As it is demonstrated in Ref. 57, a good estimate ($\phi_{measured}$) of the quantum yield, defined as the ratio between the emitted (I_{Fluo}) and the absorbed (I_{Abs}) light intensities, can be calculated from the R_f and R_{wof} values measured at the (dye) nanopigment absorption wavelength λ_0, i.e.

$$\phi_{measured} = \frac{I_{Fluo}}{I_{Abs}} = \frac{R_{wof}(\lambda_0) - R_f(\lambda_0)}{[R_{sub}(\lambda_0) - R_f(\lambda_0)] \times \left\{ f_S - \frac{f_{S,T}[1 - R_{wof}(\lambda_0)]}{[1 - R_f(\lambda_0)]} \right\}}, \quad (1)$$

where R_{sub} is the DR of the bare cellulose substrate, and f_S and $f_{S,T}$ are the correction factors that take into account the spectral response of the detector and the residual transmission through the cut-on filter

$$f_S = \frac{\int_\lambda I_F(\lambda) \times S(\lambda) d\lambda}{\int_\lambda I_F(\lambda) d\lambda}, \quad (2)$$

$$f_{S,T} = \frac{\int_\lambda I_F(\lambda) \times S(\lambda) \times T(\lambda) d\lambda}{\int_\lambda I_F(\lambda) d\lambda}, \quad (3)$$

with $I_F(\lambda)$, $S(\lambda)$, and $T(\lambda)$ corresponding to the steady-state fluorescence spectrum, the photodetector spectral efficiency, and the filter residual transmission spectrum, respectively (Fig. 6).

We remark that Eq. (1) yields a good approximation of the real quantum yield ϕ (i.e., $\phi_{measured} \approx \phi$) only if the cut-on filter has a negligible transmission, i.e., when $f_{S,T} \ll 1$. However, since in a generic optical setup the used filters are often characterized by a significant residual transmission

at certain emission wavelengths (i.e., $f_{S,T}<1$, see Fig. 6), a further correction is necessary. In particular, if R is the substrate DR in absence of any fluorescence (e.g., for a perfect cut-on filter), we can write R_f and R_{wof} as

$$R_{wof} = R + (1-R) f_{dye} \phi f_S, \tag{4}$$

$$R_f = R + (1-R) f_{dye} \phi f_{S,T}, \tag{5}$$

with f_{dye} corresponding to the fraction of the absorbed photons that excite the (dye) nanopigment at the excitation wavelength λ_0. Thus, combining Eqs. (4) and (5) yields

$$\phi = \frac{R_{wof} - R_f}{f_{S,T}(R_{wof}-1) f_S (R_f - 1)} \times \frac{1}{f_{dye}}, \tag{6}$$

and the photon fraction f_{dye} can be indeed obtained from the following energy conservation relation:

$$1 = R_f - F' + A_{sub} + A_{dye}, \tag{7}$$

where F' is the residual fluorescence passing through the cut-on filter, i.e.,

$$F' = (1-R) f_{dye} \phi f_{S,T}, \tag{8}$$

and A_{sub} and A_{dye} are the fractions of the incident light absorbed by the substrate and the (dye) nanopigment, respectively, i.e.,

$$A_{sub} = 1 - R_{sub}, \tag{9}$$

$$A_{dye} = f_{dye}(1-R). \tag{10}$$

Therefore, using Eqs. (8)–(10) in Eq. (7), we obtain

$$f_{dye} = \frac{(R_{sub} - R_f) + (1-R) f_{dye} \phi f_{S,T}}{(1-R)} \tag{11}$$

and, from Eq. (6)

$$\phi = \frac{(R_{wof} - R_f)(1-R)(1-\phi f_{S,T})}{(1-R_f)(R_{sub}-R_f)\left(f_S - f_{S,T}\dfrac{1-R_{wof}}{1-R_f}\right)}. \tag{12}$$

Note that, on one hand, for $f_{S,T} \ll 1$ or, equivalently, $R_f \approx R$

$$f_{dye} = \frac{(R_{sub}-R_f)}{(1-R)} \approx \frac{(R_{sub}-R_f)}{(1-R_f)} \tag{13}$$

and Eq. (12) reduces to Eq. (1), i.e.,

$$\phi = \frac{(R_{wof} - R_f)(1-R)}{(1-R_f)(R_{sub}-R_f)\left(f_S - f_{S,T}\dfrac{1-R_{wof}}{1-R_f}\right)}$$

$$= \frac{(1-R)}{(1-R_f)} \phi_{measured} \approx \phi_{measured}. \tag{14}$$

On the other hand, when $f_{S,T}<1$ (i.e., $R_f > R$), by combining Eqs. (12) and (14), we can easily estimate the real quantum yield ϕ from the measured value $\phi_{measured}$

$$\phi = \frac{\phi_{measured}}{1 + f_{S,T}\phi_{measured}}. \tag{15}$$

In Fig. 7, the *real* quantum yield ϕ is plotted as a function of $\phi_{measured}$ for $f_{S,T}$=0.0, 0.1, 0.3, and 0.5. We observe that, if

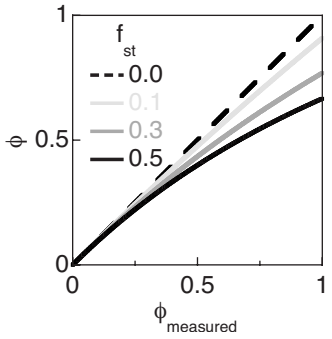

FIG. 7. Real quantum yield values (ϕ) as a function of the *measured* values ($\phi_{measured}$) for $f_{S,T}$=0–0.5 [see Eqs. (3) and (15)].

for quantum yields lower than 0.2, $\phi \approx \phi_{measured}$ independently from the used filter (i.e., from the $f_{S,T}$ value), for values larger than 0.2, $\phi_{measured}$ overestimates the real ϕ when $f_{S,T}>0.2$. Moreover, this discrepancy further increases with increasing the quantum yield and the $f_{S,T}$ values. In our case, the transmission spectrum of the cut-on filter (see Fig. 6) yields $f_{S,T}$=0.3–0.35 and Eq. (15) must be used to estimate the real ϕ values. Note that, since it is not always possible to find filters that can perfectly match the emission properties of the studied fluorescent nanopigments, having a precise correction of the experimental data that accounts for the residual filter transmission is fundamental to obtain reliable and precise quantum yield values.

Finally, we remark that, if self-absorption effects are important [e.g., when the Stokes shift is small, as for our ZL–P and PMMA–L nanopigments (see Figs. 2 and 3)], the fluorescence spectrum I_{Fluo} can be strongly affected by variations in the nanopigment concentration in the cellulose substrates. The Birk equation can then be used to correct the ϕ value and to obtain the *absolute* quantum yield ϕ_{cor}, i.e.,[57,68,69]

$$\phi_{cor} = \frac{\phi}{1 - \alpha(1-\phi)}, \tag{16}$$

where the self-absorption probability α is calculated by dividing the integrated area of the steady-state emission spectrum by the corresponding area of the emission spectrum measured for a very low (dye) nanopigment concentration in the cellulose substrate (i.e., for almost negligible self-absorption). To this purpose, the emission spectra were normalized at a wavelength where they are not affected by self-absorption (i.e., λ=600 nm, see Figs. 2 and 3).

In order to validate this technique, we measured the quantum yield of a well-known fluorescence standard. Rhodamine 101 (Fluka, purum) was chosen for its very large quantum yield (i.e., ≈1) in almost all possible configurations.[57,70] We applied the analysis procedure described above to DR measurements on Rhodamine 101 molecules adsorbed onto cellulose substrates obtaining the *absolute* value $\phi_{cor}=0.95\pm0.07$ that agrees very well with the data reported in Ref. 57.

V. RESULTS AND DISCUSSION

The DR spectra of cellulose substrates loaded with ZL–P nanopigments were measured for several concentrations, i.e.,

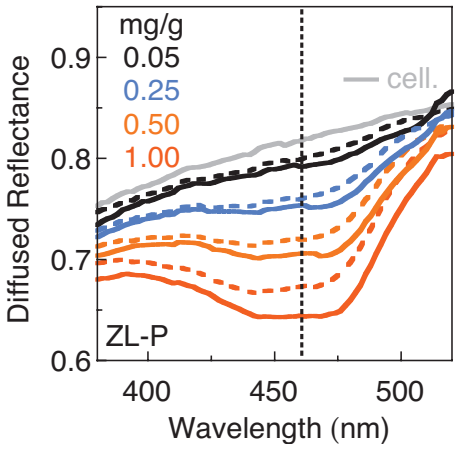

FIG. 8. (Color) Diffused reflectance spectra measured with (R_f: solid line) and without (R_{wof}: dotted line) a cut-on filter in front of the detector for the bare cellulose substrate (R_{sub}: gray line) and substrates containing ZL–P nanopigments with varying concentrations (0.05–1.00 mg/g). The absorption wavelength λ_{ABS}=460 nm is indicated (vertical dotted line).

0.05, 0.25, 0.50, and 1.00 mg/g. R_f (solid lines), R_{wof} (dotted lines), and R_{sub} (gray line) spectra are shown in Fig. 8. As it was described above, the decrease in the DR signal for the loaded substrates with respect to the bare cellulose is due to the nanopigment absorption between 400 and 500 nm (see Fig. 2) and it is stronger when the cut-on filter is used (solid lines) since this latter prevents the fluoresced photons from being detected. In order to quantify their quantum yield, the values of R_f, R_{wof}, and R_{sub} measured at the absorption wavelength λ_{ABS}=460 nm were used to calculate I_{Fluo} and I_{Abs} according to Eqs. (1)–(3) for the different ZL–P concentrations. As it is shown in Fig. 9, I_{Fluo} increases linearly with I_{Abs} as the pigment concentration increases and, even at the largest concentration values, no deviation from such linearity is observed. From the linear fit of I_{Fluo} as a function of I_{Abs}, the value $\phi_{measured}=0.35\pm0.04$ is obtained. According to Eq. (15), this yields $\phi=0.31\pm0.04$, that with Eq. (16), gives the *absolute* quantum yield $\phi_{cor}=0.37\pm0.04$.

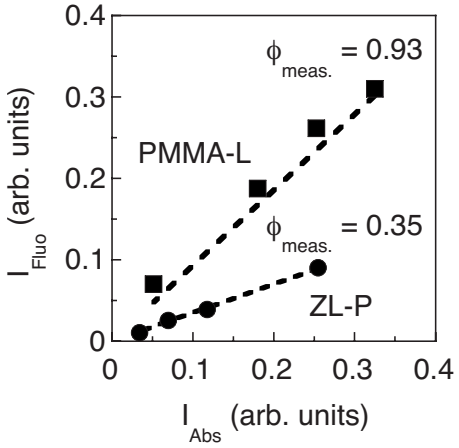

FIG. 9. Fluorescence intensity $\{I_{Fluo}=(R_{wof}-R_f)/[f_S-f_{S,T}(1-R_{wof})/(1-R_f)]\}$ as a function of the nanopigment absorption $[I_{Abs}=R_{sub}-R_f]$ for different concentrations of the ZL–P (circles) and the PMMA–L (squares) nanopigments (0.05–1.00 mg/g and 1.5–40 mg/g, respectively: see Fig. 4) adsorbed onto the cellulose substrates. The $\phi_{measured}$ values given by the linear fit (black dotted lines) are indicated.

In order to confirm this latter result and, more in general, to validate the applicability of our DR analysis to the measurement of the quantum yield of fluorescent nanopigments, we estimated the quantum yield of our ZL–P nanoparticles by means of an alternative DR method proposed by Rohwer and Martin.[58] The attenuated output of an Argon ion laser (Spectra-Physics, mod. Stalilite 2017) set at λ=458 nm was used to excite the fluorescence of the ZL–P nanopigments adsorbed onto the cellulose substrates. DR spectra were measured both with or without the fluorescent samples mounted on the integrating sphere, and alternatively placing two different filters in front of a power-meter (UDT Instrument 371 equipped with a calibrated photodiode by Graseby Optronics). These filters were used to cut-off and cut-on either the excitation or the fluorescence signal, thus enabling the measurement of both the emitted and the absorbed light powers P_{abs} and P_{em}, respectively. As in our analysis, we had to correct the measured spectra to take into account the residual transmission of the cut-on filter and the fluorescence of the cut-off filter. Following Ref. 58, we can write:

$$P_{abs}=P_{beam}\left[\frac{P_{ex}^{sub}-P_{ex}^{sub+sample}}{P_{ex}^{0}-P_{ex}^{b}}\right], \tag{17}$$

where P_{beam} is the incoming beam power, measured with the calibrated photodiode. P_{ex}^{sub} is the excitation power measured with the cut-on filter in front of the photodiode when a bare cellulose substrate is placed in the sample holder. P_{ex}^{0} and P_{ex}^{b} are the background signals measured in presence of the cut-on filter with the excitation beam on and off, respectively, when simple barium sulfate ($BaSO_4$) is contained in the sample holder. We observe that, once the cellulose substrate is loaded with the fluorescent nanopigment the excitation power can be rewritten as

$$P_{ex}^{sub+fluo}=\frac{P_{ex(measured)}^{sub+fluo}-f_{S,T}\left[(P_{em}^{sub+fluo}-P_{em}^{b})+\dfrac{P_{ex}^{b}(P_{em}^{sub}-P_{em}^{b})}{P_{ex}^{sub}-P_{ex}^{b}}\right]}{1-f_{S,T}\dfrac{P_{em}^{sub}-P_{em}^{b}}{P_{ex}^{sub}-P_{ex}^{b}}} \tag{18}$$

where $P_{ex(measured)}^{sub+fluo}$ is the measured value, while $f_{S,T}$ is the correction factor that takes into account the residual transmission through the cut-on filter. $P_{em}^{sub+fluo}$ and P_{em}^{sub} are the emission power values measured with the cut-off filter in front of the photodiode for the cellulose substrate with and without the fluorescent nanopigment, respectively. P_{em}^{b} is the background emission power measured with the excitation beam off. Finally, we can write the total emitted power as

$$P_{em}=S\left[(P_{em}^{sub+fluo}-P_{em}^{b})-(P_{em}^{sub}-P_{em}^{b})\frac{P_{ex}^{sub+fluo}-P_{ex}^{b}}{P_{ex}^{sub}-P_{ex}^{b}}\right] \tag{19}$$

with

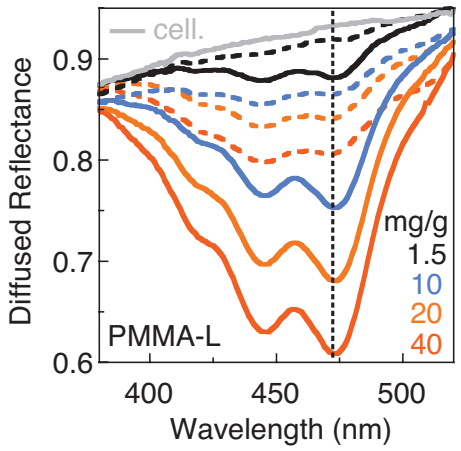

FIG. 10. (Color) DR spectra measured with (R_f: solid line) and without (R_{wof}: dotted line) a cut-on filter in front of the detector for the bare cellulose substrate (R_{sub}: gray line) and substrates containing PMMA-L nanopigments with varying concentrations (1.5–40 mg/g). The absorption wavelength $\lambda_{ABS}=470$ nm is indicated (vertical dotted line).

$$S = \frac{\int P(\lambda)d\lambda}{\int E(\lambda)P(\lambda)d\lambda}, \tag{20}$$

where $E(\lambda)$ and $P(\lambda)$ are the spectral integrating sphere efficiency and the pigment emission power (measured with the fluorimeter), respectively. Dividing P_{em} by P_{abs} yields the radiant efficiency and thus the quantum yield value.[58] In particular, for our ZL–P nanopigments Eqs. (17)–(20) yield the quantum yield value $\phi_P=0.33\pm0.7$ that agrees very well with the corresponding value $\phi_{cor}=0.37\pm0.04$ obtained with our DR technique. We highlight that, while the method by Rohwer and Martin[58] is based on the measurement of a single sample (i.e., a single nanopigment concentration in the cellulose substrate), in our procedure the quantum yield stems from the linear fit of the measurements performed on several samples, i.e., for several nanopigment concentrations taken in the linear region where self-absorption effects are small [i.e., where the correction of Eq. (16) is valid].

Finally, as for the ZL–P nanoparticles, the DR spectra of the PMMA–L nanopigments adsorbed on cellulose substrates were measured for several concentrations, i.e., 1.5, 10, 20, and 40 mg/g. R_f (solid lines), R_{wof} (dotted lines), and R_{sub} (gray line) spectra are shown in Fig. 10. Note that the difference between the measured R_f and R_{wof} spectra is much larger than in Fig. 8, thus showing qualitatively a larger quantum yield for the PMMA–L nanoparticles than for the ZL–P nanopigments. The diffuse reflectance values R_f, R_{wof}, and R_{sub} at the absorption wavelength $\lambda_{ABS}=470$ nm were used to calculate I_{Fluo} and I_{Abs} according to Eqs. (1)–(3) for the different PMMA–L contents. As for ZL–P, even at the highest concentration values, no deviation from the linearity is observed (see Fig. 9). The linear fit of I_{Fluo} as a function of I_{Abs} yields $\phi_{measured}=0.93\pm0.05$. With Eqs. (15) and (16), this yields $\phi=0.70\pm0.05$ and $\phi_{cor}=0.74\pm0.05$, respectively.

We observe that, while the quantum yield of nondeoxygenate PDB solutions in ethanol measured using a standard procedure and taking fluorescein as reference is 0.9,[71,72] our results clearly show that the latter value is more than halved once the PDB molecules have been infiltrated into the zeolite nanoparticles (see Ref. 60 for more details). The same decrease in the quantum yield with respect to the dye in solution is found for the PMMA–L nanopigments. If the quantum yield of LY83 solutions in toluene measured using a standard procedure is 0.9,[66] this value decreases by 15%–20% once the LY83 molecules have been infiltrated into the PMMA nanospheres. Although in this latter case the fluorescence efficiency might be slightly affected by the presence of a very small quantity of residual aggregates in the doped PMMA–L nanospheres (as it is revealed by their emission spectra:,see above, Fig. 3), it is evident that the nanopigment quantum yield is strongly affected by the dye encapsulation, i.e., by the physical-chemical interactions between the molecules and the host environment. In order to thoroughly understand the results obtained for our ZL–P and PMMA–L nanopigments, a systematic and comparative study of the factors that may differently affect the quantum yield of these inorganic-organic and organic-organic nanopigments would be necessary. Nevertheless, that would go beyond the objectives of this article, whose aim is simply to provide a precise and reliable technique for the measurement of the nanopigment quantum yield.

VI. CONCLUSION

In conclusion, a precise and direct DR technique was presented for the quantitative assessment of the *absolute* quantum yield of fluorescent nanopigments. This experimental method was thoroughly validated and successively applied to inorganic zeolite and organic PMMA nanoparticles loaded with fluorescent perylene molecules. Reliable quantum yield values were obtained for both low- and high-quantum efficiency nanopigments, i.e., for ZL–P and PMMA–L, respectively. We observe that our technique is not based on a single measurement of a single sample, but the quantum yield is obtained from the linear fit of several experimental data yielded by the differential DR measurements (with and without a cut-on filter) of several samples with varying fluorofor concentrations. Therefore, this method can be applied for the measurement of a very large palette of quantum yield values, provided that the difference between the DR signals with and without the filter is not negligible, i.e., the fluorescence signal is larger than the cellulose diffuse reflectance. When measuring fluorescent nanopigments with a very low quantum yield or dye concentration, the technique will work well if the fluorescence signal can be increased by increasing the nanopigment concentration in the cellulose, provided that the linear dependence of fluorescence versus absorption is preserved.

We highlight that in the domain of hybrid nanopigments there is a need to advance in establishing how encapsulation influences the emission of an incorporated guest. Therefore, a reliable measurement of the quantum yield of nanopigments is fundamental for the fabrication and development of new inorganic-organic and organic-organic fluorescent materials. Eventually, this article provides researchers studying encapsulated functional nanopigments with a powerful and

simple experimental technique for the quantitative investigation of the quantum yield of fluorescent nanopigments as a function of different system parameters.

ACKNOWLEDGMENTS

This work was supported by the Swiss Confederation Innovation Promotion Agency (Commission pour la Technologie et l'Innovation—CTI) and the Swiss National Science Foundation (SNSF) through the Grant Nos. CTI-8184.1 EPRP-IW and SNSF-200021-111856 projects, respectively.

[1]X. Michalet, F. Pinaud, T. D. Lacoste, M. Dahan, M. P. Bruchez, A. P. Alivisatos, and S. Weiss, Single Mol. **2**, 261 (2001).
[2]G. Calzaferri, S. Huber, H. Mass, and C. Minkowski, Angew. Chem., Int. Ed. **42**, 3732 (2003).
[3]P. Sharma, S. Brown, G. Walter, S. Santra, and B. Moudgil, Adv. Colloid Interface Sci. **123–126**, 471 (2006).
[4]L. Zhao, Z. Lei, X. Li, S. Li, J. Xu, B. Peng, and W. Huang, Chem. Phys. Lett. **420**, 480 (2006).
[5]R. Kinderman, L. H. Slooff, A. R. Burgers, N. J. Bakker, A. Büchtemann, R. Danz, and J. A. M. van Roosmalen, ASME J. Sol. Energy Eng. **129**, 277 (2007).
[6]R. Asakura, I. Kusayama, D. Saito, T. Isobe, K. Kurokawa, Y. Hirayama, H. Aizawa, T. Takagi, and M. Ohkubo, Jpn. J. Appl. Phys., Part 1 **46**, 5193 (2007).
[7]W. Chen, J. Nanosci. Nanotechnol. **8**, 1019 (2008).
[8]P. Uthirakumar, Y.-S. Lee, E.-K. Suh, and C.-H. Hong, J. Lumin. **128**, 287 (2008).
[9]J. Schneider, D. Fanter, M. Bauer, C. Schomburg, D. Wöhrle, and G. Schulz-Ekloff, Microporous Mesoporous Mater. **39**, 257 (2000).
[10]N. Tessler, V. Medvedev, M. Kazes, S.-H. Kan, and U. Banin, Science **295**, 1506 (2002).
[11]C. Sanchez, B. Lebeau, F. Chaput, and J.-P. Boilot, Adv. Mater. **15**, 1969 (2003).
[12]I. Gourevich, H. Pham, J. E. N. Jonkman, and E. Kumacheva, Chem. Mater. **16**, 1472 (2004).
[13]G. Calzaferri, S. Huber, A. Deveaux, A. Z. Ruiz, H. Li, O. Bossart, and L.-Q. Dieu, Proc. SPIE **6192**, 619216 (2006).
[14]S. Suárez, A. Devaux, J. Bañuelos, O. Bossart, A. Kunzmann, and G. Calzaferri, Adv. Funct. Mater. **17**, 2298 (2007).
[15]G. Schulz-Ekloff, D. Wöhrle, B. van Duffel, and R. A. Schoonheydt, Microporous Mesoporous Mater. **51**, 91 (2002).
[16]E. Johansson, E. Choi, S. Angelos, M. Liong, and J. I. Zink, J. Sol-Gel Sci. Technol. **46**, 313 (2008).
[17]F. Tronc, M. Li, J. Lu, M. A. Winnik, B. Lal Kaul, and J.-C. Graciet, J. Polym. Sci., Part A: Polym. Chem. **41**, 766 (2003).
[18]Z. Hu, Q. Zhang, M. Xue, Q. Sheng, and Y.-G. Liu, Opt. Mater. **30**, 851 (2008).
[19]T. Tamai, M. Watanabe, H. Maeda, and K. Mizuno, J. Polym. Sci., Part A: Polym. Chem. **46**, 1470 (2008).
[20]M. L. Cano, V. Fornés, H. García, M. A. Miranda, and G. Pérez-Prieto, J. Chem. Soc., Chem. Commun. **1995**, 2477.
[21]H. García, S. García, G. Pérez-Prieto, and J. C. Scaiano, J. Phys. Chem. **100**, 18158 (1996).
[22]M. Pauchard, A. Devaux, and G. Calzaferri, Chem.-Eur. J. **6**, 3456 (2000).
[23]H. Gao, Y. Zhao, S. Fu, B. Li, and M. Li, Colloid Polym. Sci. **280**, 653 (2002).
[24]M. Takasu, T. Shiroya, K. Takeshita, M. Sakamoto, and H. Kawaguchi, Colloid Polym. Sci. **282**, 740 (2004).
[25]K. Ando and H. Kawaguchi, J. Colloid Interface Sci. **285**, 619 (2005).
[26]M. A. Keane, Opt. Mater. **138**, 11 (1998).
[27]A. Corma and H. Garcia, Eur. J. Inorg. Chem. **2004**, 1143.
[28]D. Brühwiler and G. Calzaferri, Microporous Mesoporous Mater. **72**, 1 (2004).
[29]U. Vietze, O. Krauss, F. Laeri, G. Ihlein, F. Schüth, B. Limburg, and M. Abraham, Phys. Rev. Lett. **81**, 4628 (1998).
[30]I. Braun, G. Ihlein, F. Laeri, J. U. Nöckel, G. Schulz-Ekloff, F. Schüth, U. Vietze, Ö. Weiss, and D. Wöhrle, Appl. Phys. B: Lasers Opt. **70**, 335 (2000).
[31]Ö. Weiß, J. Loerke, U. Wüstefeld, F. Marlow, and F. Schüth, J. Solid State Chem. **167**, 302 (2002).
[32]C.-Y. Mou and H. P. Lin, Pure Appl. Chem. **72**, 137 (2000).
[33]M. Ganschow, M. Wark, D. Wöhrle, and G. Schulz-Ekloff, Angew. Chem. **112**, 167 (2000).
[34]T. Martin, A. Galarneau, F. Di Renzo, F. Fajula, and D. Plee, Angew. Chem., Int. Ed. **41**, 2590 (2002).
[35]I. Sokolov, Y. Y. Kievsky, and J. M. Kaszpurenko, Small **3**, 419 (2007).
[36]W. Stöber, A. Fink, and E. Bohn, J. Colloid Interface Sci. **26**, 62 (1968).
[37]A. P. Philipse and A. Vrij, J. Colloid Interface Sci. **128**, 121 (1989).
[38]X. Zhao, R. P. Bagwe, and W. Tan, Adv. Mater. **16**, 173 (2004).
[39]M. Montalti, L. Prodi, N. Zaccheroni, A. Zattoni, P. Reschiglian, and G. Falini, Langmuir **20**, 2989 (2004).
[40]J. Fölling, S. Polyakova, V. Belov, A. van Blaederen, M. L. Bossi, and S. W. Hell, Small **4**, 134 (2008).
[41]M. Antonietti and K. Tauer, Macromol. Chem. Phys. **204**, 207 (2003).
[42]See, for example, http://www.neomark.com.tw/index.html
[43]W. R. Bergmark, A. Davis, C. York, A. Macintosh, and G. Jones, J. Phys. Chem. **94**, 5020 (1990).
[44]J. Mohanty and W. M. Nau, Angew. Chem., Int. Ed. **44**, 3750 (2005).
[45]J. R. Lakowicz, *Principles of Fluorescence Spectroscopy* (Kluwer Academic-Plenum, New York, 1999).
[46]A. T. R. Williams, S. A. Winfield, and J. N. Miller, Analyst (Cambridge, U.K.) **108**, 1067 (1983).
[47]S. Dhami, A. J. De Mello, G. Rumbles, S. M. Bishop, D. Phillips, and A. Beeby, Photochem. Photobiol. **61**, 341 (1995).
[48]B.-K. An, S.-K. Kwon, S.-D. Jung, and S. Y. Park, J. Am. Chem. Soc. **124**, 14410 (2002).
[49]H. Maeda, T. Maeda, K. Mizuno, K. Fujimoto, H. Shimizu, and M. Inouye, Chem.-Eur. J. **12**, 824 (2006).
[50]V. Pilla, L. P. Alves, E. Munin, and M. T. T. Pacheco, Opt. Commun. **280**, 225 (2007).
[51]M. Alvaro, H. Garcia, S. Corrent, and J. C. Scaiano, J. Phys. Chem. B **102**, 7530 (1998).
[52]Y. Kawamura, H. Sasabe, and C. Adachi, Jpn. J. Appl. Phys., Part 1 **43**, 7729 (2004).
[53]C. Norakankorn, Q. Pan, G. L. Rempel, and S. Kiatkamjornwong, Macromol. Rapid Commun. **28**, 1029 (2007).
[54]A. D. Dinsmore, E. R. Weeks, V. Prasad, A. C. Levitt, and D. A. Weitz, Appl. Opt. **40**, 4152 (2001).
[55]A. Herrmann and K. Müllen, Chem. Lett. **35**, 978 (2006).
[56]S. A. Ruetten and L. K. Thomas, J. Phys. Chem. B **102**, 598 (1998).
[57]L. F. V. Ferreira, T. J. F. Branco, and A. M. B. Do Rego, ChemPhysChem **5**, 1848 (2004).
[58]L. S. Rohwer and J. E. Martin, J. Lumin. **115**, 77 (2005).
[59]A.Z. Ruiz, D. Brühwiler, T. Ban, and G. Calzaferri, Monatsch. Chem. **136**, 77 (2005).
[60]O. Nicolet, S. Huber, C. Lovey, S. Chappellet, J. Perrenoud, M. Pauchard, R. Ferrini, and L. Zuppiroli, Adv. Funct. Mater. **19**, 1877 (2009).
[61]http://shop.abcr.de/product_information.aspx?product_id=40781&second_id=138958
[62]S. Hashimoto, M. Hagiri, N. Matsubara, and S. Tobita, Phys. Chem. Chem. Phys. **3**, 5043 (2001).
[63]S. Huber and G. Calzaferri, ChemPhysChem **5**, 239 (2004).
[64]H. Maas, A. Kathyr, and G. Calzaferri, Microporous Mesoporous Mater. **65**, 233 (2003).
[65]D. Allard, B. Lange, F. Fleischhaker, R. Zentel, and M. Wulf, Soft Mater. **3**, 121 (2005).
[66]http://www.basf.com/additives/pdfs/lumyel083.pdf
[67]L. F. V. Ferreira, J. C. Netto-Ferreira, I. Khmelinskii, A. R. Garcia, and S. M. B. Costa, Langmuir **11**, 231 (1995).
[68]F. Wilkinson, P. A. Leicester, L. F. V. Ferreira, and V. M. R. Freire, Photochem. Photobiol. **54**, 599 (1991).
[69]M. G. Lagorio, L. E. Dicelio, M. I. Litter, and H. San Roman, J. Chem. Soc., Faraday Trans. **94**, 419 (1998).
[70]L. F. V. Ferreira, M. R. Freixo, A. R. Garcia, and F. Wilkinson, J. Chem. Soc., Faraday Trans. **88**, 15 (1992).
[71]See *A guide to recording fluorescence quantum yield* at http://www.jobinyvon.com.
[72]A. Pardo, D. Reyman, J. M. L. Poyato, and F. Medina, J. Lumin. **51**, 269 (1992).